AGU PUBLICATIONS

Paleoceanography

RESEARCH ARTICLE
10.1002/2015PA002877

Key Points:
- TEX_{86}^{L}-based SST records cover the full glacial-Holocene transition
- Controls on North Pacific and the Bering Sea SST differ prior to 15.5 ka B.P.
- Alaskan Stream causes regional differences in North Pacific climate change

Correspondence to:
V. D. Meyer,
vera.meyer@awi.de

Citation:
Meyer, V. D., L. Max, J. Hefter, R. Tiedemann, and G. Mollenhauer (2016), Glacial-to-Holocene evolution of sea surface temperature and surface circulation in the subarctic northwest Pacific and the Western Bering Sea, *Paleoceanography*, *31*, 916–927, doi:10.1002/2015PA002877.

Received 1 SEP 2015
Accepted 13 JUN 2016
Accepted article online 15 JUN 2016
Published online 6 JUL 2016

Glacial-to-Holocene evolution of sea surface temperature and surface circulation in the subarctic northwest Pacific and the Western Bering Sea

Vera D. Meyer[1,2], Lars Max[1], Jens Hefter[1], Ralf Tiedemann[1], and Gesine Mollenhauer[1,2]

[1]Alfred Wegener Institute Helmholtz Centre for Polar and Marine Research, Bremerhaven, Germany, [2]Department of Geosciences, University of Bremen, Bremen, Germany

Abstract It has been proposed that North Pacific sea surface temperature (SST) evolution was intimately linked to North Atlantic climate oscillations during the last glacial-interglacial transition. However, during the early deglaciation and the Last Glacial Maximum, the SST development in the subarctic northwest Pacific and the Bering Sea is poorly constrained as most existing deglacial SST records are based on alkenone paleothermometry, which is limited prior to 15 ka B.P. in the subarctic North Pacific realm. By applying the TEX_{86}^{L} temperature proxy we obtain glacial-Holocene-SST records for the marginal northwest Pacific and the Western Bering Sea. Our TEX_{86}^{L}-based records and existing alkenone data suggest that during the past 15.5 ka, SSTs in the northwest Pacific and the Western Bering Sea closely followed millennial-scale climate fluctuations known from Greenland ice cores, indicating rapid atmospheric teleconnections with abrupt climate changes in the North Atlantic. Our SST reconstructions indicate that in the Western Bering Sea SSTs drop significantly during Heinrich Stadial 1 (HS1), similar to the known North Atlantic climate history. In contrast, progressively rising SST in the northwest Pacific is different to the North Atlantic climate development during HS1. Similarities between the northwest Pacific SST and climate records from the Gulf of Alaska point to a stronger influence of Alaskan Stream waters connecting the eastern and western basin of the North Pacific during this time. During the Holocene, dissimilar climate trends point to reduced influence of the Alaskan Stream in the northwest Pacific.

1. Introduction

During the last deglaciation, the North Pacific (N-Pacific) and its marginal seas experienced millennial-scale climate oscillations, which are proposed to be linked to variations in the strength of the Atlantic Meridional Overturning Circulation (AMOC) [e.g., *Seki et al.*, 2002; *Kiefer and Kienast*, 2005; *Gebhardt et al.*, 2008; *Harada et al.*, 2012; *Max et al.*, 2012; *Kuehn et al.*, 2014]. It has been proposed that AMOC weakened twice during the last deglaciation (Heinrich Stadial 1 and Younger Dryas stadials) due to vast freshwater supply from melting continental ice sheets into the N-Atlantic, which lead to abrupt cooling in the N-Atlantic realm [e.g., *McManus et al.*, 2004]. Proxy-based SST reconstructions as well as general circulation models (GCM) lead to an inconsistent picture regarding the N-Pacific response and the underlying teleconnection. Some studies (based on climate models and proxy data) found an out-of-phase behavior with cooling in the N-Atlantic and a concurrent warming in the N-Pacific during stadials [*Sarnthein et al.*, 2004, 2006; *Gebhardt et al.*, 2008]. It has been proposed that the weakening of the AMOC would result in the establishment of a Pacific Meridional Overturning Circulation and hence intensified poleward heat transport in the N-Pacific [*Schmittner et al.*, 2003; *Saenko et al.*, 2004; *Okazaki et al.*, 2010; *Menviel et al.*, 2012]. By contrast, several GCMs suggested an in-phase behavior of the N-Pacific and N-Atlantic climates, which was attributed to rapid atmospheric teleconnections connecting both oceans [*Mikolajewicz et al.*, 1997; *Vellinga and Wood*, 2002; *Okumura et al.*, 2009; *Timmermann et al.*, 2010; *Chikamoto et al.*, 2012]—an idea supported by the majority of proxy-based studies from the N-Pacific [*Kienast and McKay*, 2001; *Pisias et al.*, 2001; *Barron et al.*, 2003; *Harada et al.*, 2012; *Max et al.*, 2012; *Kuehn et al.*, 2014; *Praetorius and Mix*, 2014; *Praetorius et al.*, 2015]. Still, for the early deglaciation, the SST development and its potential linkage to AMOC variations remains underconstrained since most proxy-based studies do not allow insights into the Heinrich Stadial 1 (HS1) and the Last Glacial Maximum (LGM). This is because for this time-interval alkenone paleothermometry, the tool most often applied for SST reconstructions [e.g., *Ternois et al.*, 2000; *Barron et al.*, 2003; *Caissie et al.*, 2010; *Seki et al.*, 2004a; *Kiefer and Kienast*, 2005; *Max et al.*, 2012], is afflicted by several limitations [see, e.g., *Caissie et al.*, 2010; *Max et al.*, 2012].

Specifically, alkenone concentrations are often extremely low or even below detection limit in sediments older than approximately 15–16 ka [*Ternois et al.*, 2000; *Barron et al.*, 2003; *Caissie et al.*, 2010; *Seki et al.*, 2004a; *Max et al.*, 2012], which prevents the application of $U^{K'}_{37}$ during HS1 and LGM. The growth of coccolithophorids, the alkenone producers, may have been impeded by unfavorable environmental conditions during glacial times. Besides, in records where alkenones are present (Sea of Okhotsk), they tend to produce unexpectedly warm temperatures for the last glacial period and early deglaciation, which points to a seasonal bias [e.g., *Seki et al.*, 2004b]. It has been assumed that longer-lasting sea ice seasons likely forced phytoplankton to bloom in late summer during glacial times, while under modern conditions phytoplankton blooms occur during early spring/fall [*Takahashi et al.*, 2002; *Harada et al.*, 2003; *Seki et al.*, 2004b, 2007]. Given these limitations of alkenone paleothermometry and the poor knowledge about the SST development in the subarctic N-Pacific and its potential linkage to AMOC variations during the early deglaciation, the establishment of SST records spanning the entire LGM-Holocene transition is necessary.

The TEX_{86} (Tetra Ether indeX) has been introduced as SST proxy by *Schouten et al.* [2002] and quantifies the relative abundance of isoprenoid glycerol dialcyl glycerol tetraethers (isoGDGTs) consisting of 86 C-atoms. These lipids are synthesized by marine Thaumarchaeota, planktonic ammonia oxidizing chemoautotrophes [*Könneke et al.*, 2005; *Martens-Habbena et al.*, 2009; *Walker et al.*, 2010]. While coccolithophorids bloom during early spring and fall [*Takahashi et al.*, 2002; *Harada et al.*, 2003], the highest abundances of Thaumarchaeota have been observed in winter and summer in the subarctic gyre [e.g., *Karner et al.*, 2001; *Seki et al.*, 2009, 2014; *Yamamoto et al.*, 2012]. As chemoautotrophs Thaumarchaeota have different ecological preferences than the phototrophic coccolithophorids and may not be affected by environmental stress factors, which limit the alkenone producing algae, rendering the TEX_{86} potentially useful in settings where alkenone paleothermometry is problematic.

Applying the TEX_{86} temperature proxy to two sediment cores from the Western Bering Sea and the marginal NW Pacific, we were able to produce full glacial to Holocene records in SST. Our SST data provide new insights into teleconnections between the N-Pacific and N-Atlantic during the early deglaciation and reveal new aspects about the role of oceanic surface circulation in N-Pacific climate change during the LGM-Holocene transition.

2. Regional Setting

The surface circulation in the North Pacific and the Bering Sea is cyclonic (Figure 1). At 40°N the North Pacific Current, the extension of the subtropical Kuroshio Current, flows eastward carrying warm and saline surface waters into the Alaskan Gyre/Northeast Pacific (NE Pacific). The Alaskan Stream (AS) forms a northern boundary current flowing along the Aleutian Arc into the Western Sub-polar Gyre. Through several passages of the Aleutian Islands surface waters from the AS enter the Bering Sea where they form the Aleutian North Slope Current (ANSC), a surface current flowing eastward along the Aleutian Arc. The ANSC acts as the southern boundary current of the counterclockwise circulation of the Bering Sea. In the north, the Bering Slope Current transports the water masses along the coastlines of Alaska and Siberia. The Bering Sea waters leave the Bering Sea via the Bering Strait into the Arctic Ocean. The main outflow, however, is through the Kamchatka Strait, where surface waters enter the NW Pacific via the East Kamchatka Current (EKC). The EKC flows along the eastern coast of the Kamchatka Peninsula and forms the western boundary current of the Western Sub-polar Gyre [e.g., *Stabeno and Reed*, 1994].

The N-Pacific and its marginal seas are characterized by strong seasonal contrasts in SST (winter: 0–3°C; summer: 8–12°C [*Locarnini et al.*, 2010]) and upper water column stratification. The seasonal contrasts are linked to seasonal changes of the major atmospheric circulation over the N-Pacific [e.g., *Niebauer et al.*, 1999]. During winter, the Aleutian Low develops over the N-Pacific and brings cold air masses from the Arctic to the subarctic N-Pacific. The cold air induces cooling of surface waters and sea ice formation in the Bering Sea [*Ohtani et al.*, 1972; *Niebauer et al.*, 1999]. Brine rejection as well as wind stress cause vertical mixing of surface and subsurface waters. During summer the Aleutian Low weakens and the North Pacific High establishes over the N-Pacific. This brings warm southerly winds to the subarctic N-Pacific and the Bering Sea. Together with increasing insolation this causes sea ice melt and warming of surface waters. As a consequence a distinct upper ocean stratification with pronounced seasonal pycnocline and thermocline develops [*Ohtani et al.*, 1972].

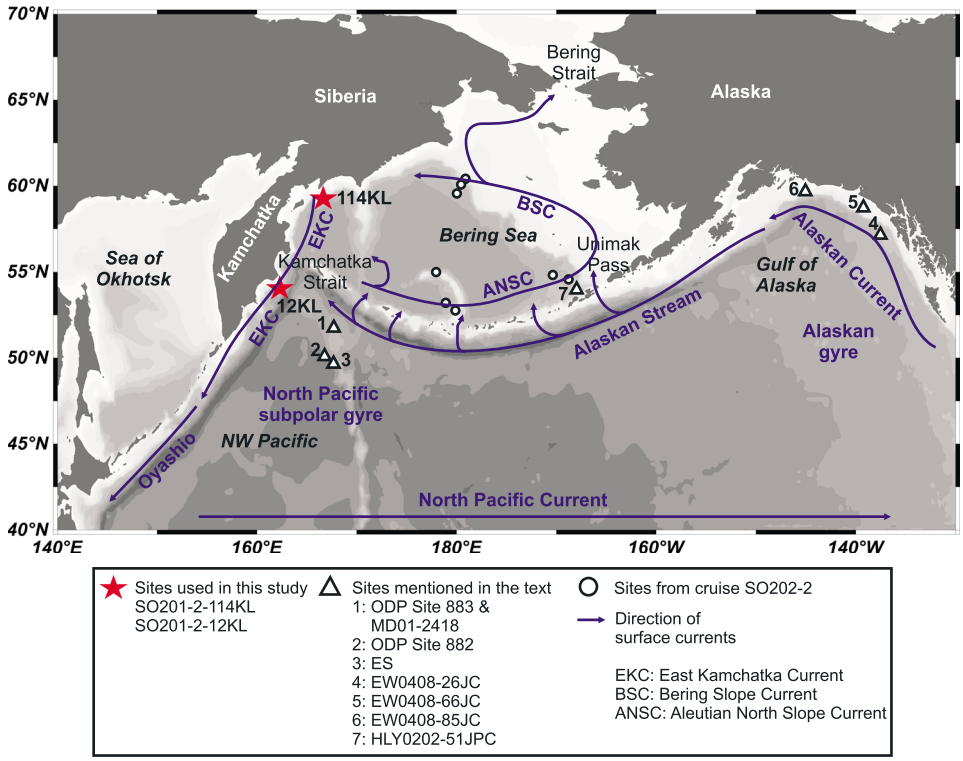

Figure 1. Map of the study area. Sites of the sediment cores used in this study are shown together with core sites from other studies mentioned in the text. Additionally, the general surface circulation pattern of the N-Pacific and the Bering Sea is sketched. The map was created using "Ocean Data View" [*Schlitzer,* 2011].

3. Material and Methods

3.1. Core Material and Age Control

For this study, we used two piston cores from the Western Bering Sea (SO201-2-114KL) and the NW Pacific (SO201-2-12KL) recovered at the continental margin off Kamchatka Peninsula (Figure 1) during Kurile-Kamchatka and Aleutian Marginal Sea Island Arc Systems (KALMAR) Leg 2, cruise of R/V SONNE SO201 in 2009 [*Dullo et al*., 2009]. Prior to sample preparation, cores were stored at 4°C. Integrated age models were developed by accelerator mass spectrometry (AMS) radiocarbon dating of planktonic foraminifera (*Neogloboquadrina pachyderma* sinistral) as well as by core-to-core correlations of high-resolution spectrophotometric (color b*) and X-ray fluorescence data. For a detailed description and AMS-^{14}C results see *Max et al.* [2012]. For this study, cores were sampled in 10 cm (12KL) and 5 cm (114KL) steps providing a temporal resolution of approximately 250–500 years. The cores have a total recovery of 11.78 m (12KL) and 7.89 m (114KL) representing the periods of 1–20 ka B.P. and 8.8–29 ka B.P..

3.2. Lipid Extraction

The sediment samples (5 g) were freeze-dried and homogenized. Ten micrograms of C_{46}-GDGT were added as internal standard. Samples were extracted with an accelerated solvent extractor (Dionex ASE 200) using 22 mL cells and dichlormethane (DCM):methanol (MeOH) 9:1 (vol/vol) as solvent at 100°C and 6.895E+6 Pa with three cycles of 5 min each. The total lipid extracts were dried with a rotary evaporator. Afterward they were hydrolyzed with 0.1 N potassium hydroxide (KOH) in MeOH:H_2O 9:1 (vol/vol). Neutral compounds (including GDGTs) were extracted with *n*-hexane. Different compound classes were separated by column chromatography, using deactivated SiO_2. An apolar fraction was eluted using *n*-hexane. Polar compound classes, including the GDGTs, were eluted with MeOH:DCM 1:1 (vol/vol). Dissolved in hexane:isopropanol 99:1 (vol/vol) the polar-fraction was filtered with a polytetrafluoroethylene filter (0.45 μm pore size) according to *Hopmans et al.* [2004]. Samples were brought to a concentration of 2 μg/μL prior to GDGT analysis.

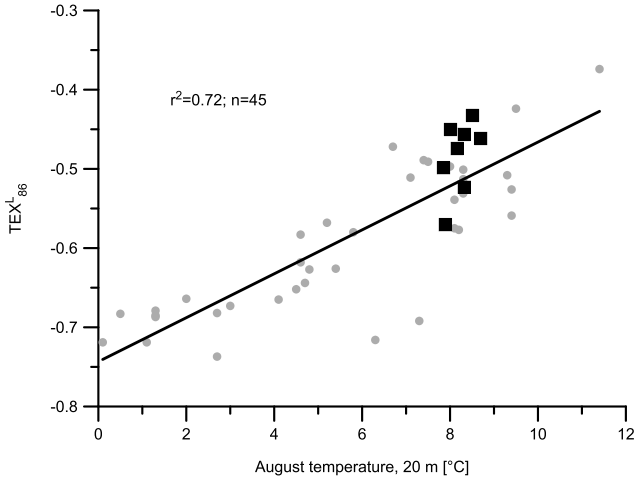

Figure 2. TEX^{L}_{86} plotted against mean August temperature in 20 m water depth in the subpolar North Pacific, the Sea of Okhotsk, and the Bering Sea. The grey dots represent the core-top data set from the northwest Pacific and the Sea of Okhotsk, on which *Seki et al.* [2014] established the regional TEX^{L}_{86} calibration. Core-top data from the Bering Sea (black squares, sites from cruise SO202-2 [*Ho et al.*, 2014]) (Figure 1) are implemented. For the Bering Sea sites the respective August water temperatures were taken from WOA09 [*Locarnini et al.*, 2010]. For the NW Pacific and the Sea of Okhotsk please see *Seki et al.* [2014, and references therein].

3.3. GDGT Analysis and SST Determination

GDGTs were analyzed by high-performance liquid chromatography coupled via an atmospheric pressure chemical ionization interface to a single quadrupole mass selective detector according to *Chen et al.* [2014]. The MS detector was set for selected-ion monitoring of the following $(M + H)^+$ ions: *m/z* 1302.3 (GDGT 0), 1300.3 (GDGT 1), 1298.3 (GDGT 2), 1296.3 (GDGT 3), 1292.3 (GDGT 4 + 4′/crenarcheol + regio-isomer), 1050 (GDGT III), 1036 (GDGT II), 1022 (GDGT I), and 744 (C_{46} standard), with a dwell time of 67 ms per ion.

Peak areas from the individual GDGTs were obtained by integration. Compounds were quantified by using the respective peak areas and the response factor of the C_{46} standard. The results were normalized to the amount of extracted sediment and total organic carbon content. We applied the TEX^{L}_{86}-index, which has been suggested as proxy for annual SST in settings where temperature ranges below 15°C by *Kim et al.* [2010]. In order to convert TEX^{L}_{86} into temperatures we applied the regional calibration for the Sea of Okhotsk and the NW Pacific by *Seki et al.* [2014]. The reported standard error for the regional calibration is ±1.7°C. The standard deviation for TEX^{L}_{86} was calculated from repeated measurements and was <0.01 corresponding to a maximal uncertainty of ±0.37°C in the reconstructed temperatures.

According to the regional calibration from *Seki et al.* [2014] TEX^{L}_{86} would reflect mean August temperatures in 20 m water depth (Figure 2). As the data set from *Seki et al.* [2014] does not include data from the Bering Sea, we tested whether the proposed regional calibration would be applicable there by combining core-top data [from *Ho et al.*, 2014] from the central Bering Sea (Figure 1, sites SO202-2) and the data set from *Seki et al.* [2014]. Since data from the Bering Sea were within the range of values from the Sea of Okhotsk/N-Pacific we concluded that the regional calibration is valid for the Bering Sea (Figure 2). *Seki et al.* [2014] argued that a highly stratified water column in summer restricted the summer warmth to 20 m and 40 m in the Sea of Okhotsk and the NW Pacific and that ammonium concentrations peaked in that depth interval at the same time. As Thaumarchaeota are ammonia oxidizing chemoautotrophs [*Könneke et al.*, 2005; *Martens-Habbena et al.*, 2009; *Walker et al.*, 2010] they probably accumulate in that depth range during the summer months [*Seki et al.*, 2014, and references therein]. Conductivity-temperature-depth profiles from the Western Bering Sea show that the development of the water column is similar to the NW-Pacific/Sea of Okhotsk with respect to the depth of summer stratification [*Dullo et al.*, 2009; *Riethdorf et al.*, 2013]. Therefore, it is reasonable to assume that ammonium may accumulate in the mixed-layer of the Bering Sea during the summer season and would be accompanied by enhanced productivity of Thaumarchaeota.

As *Weijers et al.* [2006] pointed out that terrigenous GDGTs can bias the temperature signal of TEX_{86} when terrigenous organic matter input is high, we determined the relative contribution of marine and terrigenous GDGTs in our samples using the branched and isoprenoid tetraether (BIT) index after *Hopmans et al.* [2004]. The index is based on a ratio of terrigenous GDGTs (GDGT I-III) and the marine Crenachaeol (GDGT 4). Repeated measurements resulted in a standard deviation of 0.01, which corresponds to an analytical error of ±0.004 BIT units.

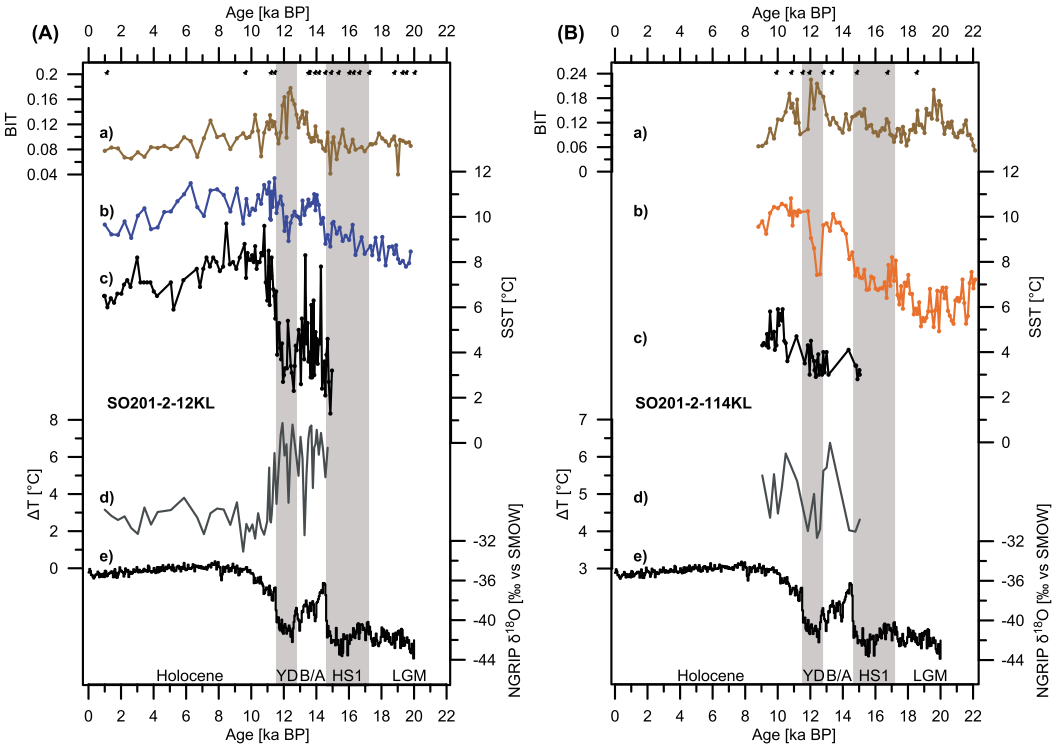

Figure 3. Sea surface temperature reconstruction and BIT-indices over the past 22 ka for the NW Pacific ((a) site 12KL) and the Western Bering Sea ((b) site 114KL). (a) BIT indices (this study), (b) TEX^{L}_{86}-based SSTs (this study), (c) $SST_{UK'37}$ [*Max et al.*, 2012], (d) $\Delta T_{TEXL86\text{-}UK'37}$, and (e) the NGRIP oxygen isotope record from Greenland ice cores [*North Greenland Ice Core Project members*, 2004] are shown to present the climate variability in the N-Atlantic. The grey shaded areas mark the YD and the HS1 stadials. The black pins mark the age-control points for cores 12KL and 114KL obtained from radiocarbon dating of *Neogloboquadrina pachyderma* (sin.) [*Max et al.*, 2012].

4. Results

4.1. BIT Values and Applicability of TEX^{L}_{86}-Based SST Reconstructions

BIT values and TEX^{L}_{86}-derived SST (SST_{TEXL86}) are shown in Figure 3, together with alkenone-based SST ($SST_{UK'37}$), which were established on the same cores by *Max et al.* [2012]. Ranging between 0.04 and 0.22, BIT values are below the critical value of 0.3, defined by *Weijers et al.* [2006], where SST reconstructions are potentially biased by terrigenous isoGDGTs (Figure 3). Hence, at sites 12KL and 114KL marine-derived GDGTs dominate over terrigenous GDGTs, making us confident that TEX^{L}_{86} is not biased by terrigenous input. At site 12KL TEX^{L}_{86}-based SST reconstructions for the core-top (1000 ka B.P., 9.5°C) match modern summer SST in the Western Subarctic Gyre (approximately 9–11°C; satellite data from WOA09 [*Locarnini et al.*, 2010]) confirming that TEX^{L}_{86} reflects summer SST. Since site 114KL does not cover the entire Holocene a comparison of late Holocene SST with modern satellite data is not possible. The TEX^{L}_{86}-derived SST from the early Holocene (10–9.5°C) gives estimates slightly above modern summer SST (approximately 8°C; WOA09 [*Locarnini et al.*, 2010]). This offset is likely because the reconstructed temperatures fall in the time period of the Holocene Thermal Maximum that occurred between 11 and 8 ka B.P. in the NW Pacific and Siberia [e.g., *Max et al.*, 2012; *Biskaborn et al.*, 2012, and references therein] and was warmer than at present, which may explain the offset.

4.2. SST Development Over the Past 22 ka

Whereas the previously published $U^{K'}_{37}$ records span the last 15 ka only [*Max et al.*, 2012], our TEX^{L}_{86} records reach back to the LGM (Figure 3). During the LGM Bering Sea SST_{TEXL86} ranges between 5°C and 7°C, while SST_{TEXL86} in the NW Pacific ranges between 8°C and 9°C. During the deglaciation SST_{TEXL86} increases about 4–5°C in the Western Bering Sea but, less in the NW Pacific (approximately 3°C, site 12KL). SST_{TEXL86} in the NW Pacific reaches maxima at 11.5 ka B.P. and 6 ka B.P.. Between the middle to late Holocene (since 8 ka B.P.)

SST_{TEXL86} is characterized by progressive long-term cooling. While a temperature offset between the Western Bering Sea and the NW Pacific of approximately 2°C is present during the early deglaciation both locations reach similar temperatures during the early Holocene Thermal Maximum (10–11°C, 10–8 ka B.P.; Figure 3).

Since approximately 15 ka B.P., the SST_{TEXL86} evolution at both sites has been in agreement with the previously published $SST_{UK'37}$ from *Max et al.* [2012] (Figure 3). It is characterized by a sharp temperature increase at the onset of the B/A and a subsequent cooling into the Younger Dryas (YD) cold spell followed by an abrupt warming into the early Holocene (Figure 3). SST_{TEXL86} is generally higher than $SST_{UK'37}$ at both sites (Figure 3). The difference ($\Delta T_{TEXL86\text{-}UK'37}$) is 6°C during the deglaciation (Figure 3). At site 12KL $\Delta T_{TEXL86\text{-}UK'37}$ is abruptly reduced by about 3–4°C at the Holocene transition, which is mainly driven by a sharp increase in $SST_{UK'37}$.

Whereas the Bering Sea and the NW Pacific have experienced similar SST developments since the B/A, they are characterized by different patterns prior to 15.5 ka B.P. (Figure 3). In the Bering Sea the SST_{TEXL86} records an early warming phase during the late glacial (18–17 ka B.P.), which is followed by a drop in SST during at 17–16 ka B.P.. Warming rebounds at approximately 15.5 ka B.P., and an abrupt increase in temperature occurs at the transition to the B/A-interstadial (14.6 ka B.P.). In the NW Pacific the early deglaciation SST_{TEXL86} deviates from SST_{TEXL86} at site 114KL (Figure 3). At site 12KL SST_{TEXL86} continuously rises between 18 and 14.6 ka B.P., without being interrupted by a cold reversal (Figure 3). At 14.6 ka an abrupt temperature increase marks the onset of the B/A-interstadial.

5. Discussion

5.1. Seasonal Differences Between Summer and Fall SST

Based on the good correspondence of regional core-top data with summer SST [*Seki et al*., 2014; *Ho et al*., 2014] (Figure 2), TEX_{86}^{L} is regarded to reflect summer SST in the N-Pacific and its marginal seas. In contrast, $U_{37}^{K'}$ is supposed to reflect late summer/fall SST today [*Harada et al*., 2003; *Seki et al*., 2007]. At site 12KL the Holocene $\Delta T_{TEXL86\text{-}Uk'37}$ (approximately 3°C) is in agreement with the thermal difference between summer and fall recorded by the satellite data of WOA09 [*Locarnini et al*., 2010]. Accordingly, the increased $\Delta T_{TEXL86\text{-}UK'37}$ (prior to 12 ka B.P.) implies that the deglacial thermal contrast between summer and fall was greater than during the Holocene (Figure 3). The temperature increase at the YD-Holocene boundary is stronger in the $SST_{UK'37}$ than in the SST_{TEXL86}, which makes the alkenones the main driver of the decrease in $\Delta T_{TEXL86\text{-}UK'37}$ (Figure 3), suggesting that the inferred growth season of alkenone producers, i.e., fall warmed more strongly than summer. This might be due to a deglacial prolongation of the summer season. Several GCMs suggest that the Aleutian Low was stronger during the LGM than during the Holocene [*Dong and Valdes*, 1998; *Shin et al*., 2003; *Yanase and Abe-Ouchi*, 2007, 2010; *Alder and Hostetler*, 2015] and that a distinct low-pressure anomaly persisted throughout the deglaciation, until approximately 12 ka B.P. [*Alder and Hostetler*, 2015]. In association with a stronger Aleutian Low northerly winds would intensify over the NW Pacific and would have enhanced the advection of cold arctic air during fall/winter. As a result, sea-surface cooling between summer and fall may have been more pronounced during the LGM/deglaciation than during the Holocene.

Although climatic explanations seem to be plausible, shifts in the production season of alkenones or isoGDGT could also account for variations in the thermal difference between the two SST proxies [e.g., *Seki et al*., 2009]. Since $SST_{UK'37}$ seem to be the main driver of the decrease in $\Delta T_{TEXL86\text{-}UK'37}$ at the YD-Holocene boundary (Figure 3) seasonal variations in the blooming season of coccolitophorids are more likely than of the Thaumarchaeota. *Riethdorf et al.* [2013] have already speculated that deglacial $SST_{UK'37}$ represent early spring instead of fall at site 12KL. As modern spring SST are lower than fall SST (WOA09 [*Locarnini et al*., 2010]) a shift from spring to fall potentially explains the decrease in $\Delta T_{TEXL86\text{-}UK'37}$ at the YD-Holocene boundary.

5.2. SST Evolution of the NW Pacific and Western Bering Sea Over the Past 22 ka

Long-term warming through the LGM-Holocene transition is evident in SST_{TEXL86} at both sites (Figure 4). This is generally is in agreement with rising summer insolation and increasing atmospheric CO_2-levels (CO_{2atm}; Figure 4), suggesting that those were important drivers. Cold conditions in the Bering Sea during the LGM is compatible with the idea of enhanced NPIW-formation in the Bering Sea through pronounced sea ice

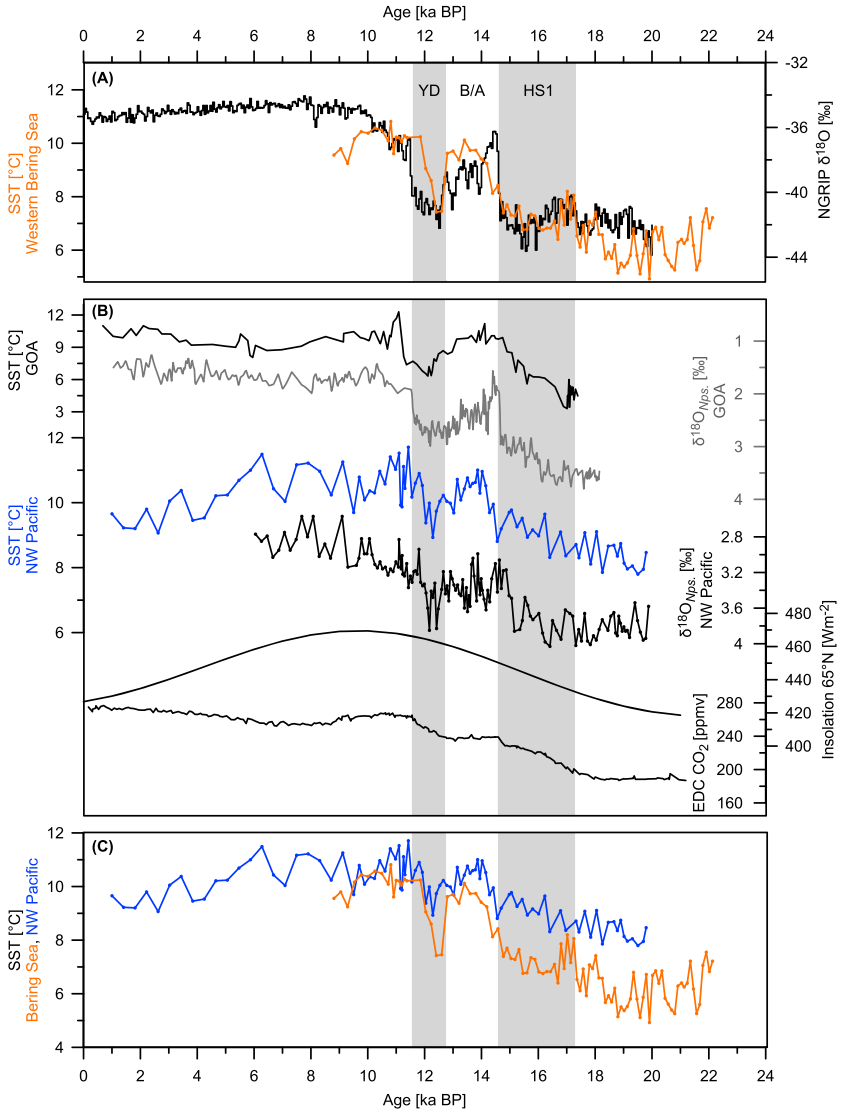

Figure 4. (a) SST_{TEXL86} from site 114KL, Western Bering Sea (orange, this study) compared to N-Atlantic climate variability represented by Greenland ice core $\delta^{18}O$ (black [*North Greenland Ice Core Project*, 2004]). (b) SST_{TEXL86} from site 12KL, NW Pacific (blue, this study) plotted together with the GOA-SST based on $U^{K'}_{37}$ (black [*Praetorius et al.*, 2015], obtained from site EW0408-85JC; see Figure 1); the GOA-$\delta^{18}O$ (grey [*Praetorius and Mix*, 2014], measured on the planktonic foraminifera *Neogloboquadrina pachyderma* (sin.) (*Nps*), obtained from sites EW0408-26JC, EW0408-85JC, and EW0408-66JC; Figure 1); the $\delta^{18}O$ measured on *Nps* from the NW Pacific/site 12KL (black [*Riethdorf et al.*, 2013]); mean July insolation at 65°N (black [*Berger and Loutre*, 1991]); and CO_{2atm} (black, Epica Dome C [*Monnin et al.*, 2001; *Parrenin et al.*, 2013]). (c) Comparison of SST_{TEXL86} from sites 12KL (blue) and 114KL (orange).

formation [*Knudson and Ravelo*, 2015]. Since the magnitude of deglacial warming in the NW Pacific is approximately 2°C smaller than in the Western Bering Sea (Figures 3 and 4) and since glacial SST (site 12KL) is only 1.5°C lower than modern, much smaller than the magnitude of the glacial cooling proposed for the subarctic N-Pacific by the MARGO-compilation (2–6°C [*Waelbroeck et al.*, 2009]), it is conceivable that local factors strongly influenced the long-term SST evolution at our core sites. In the following we discuss potential regional and supraregional influences on our records.

5.2.1. Short-Term Variability and N-Atlantic Coupling

Between 10 and 15 ka B.P. the short-term variability exhibited in SST_{TEXL86} from both settings resembles the previously published alkenone data from *Max et al.* [2012] and shows a similar pattern as recorded in North Greenland Ice Core Project (NGRIP)-$\delta^{18}O$ (Figure 3). This supports the idea of simultaneous temperature development in the N-Atlantic and the N-Pacific caused by atmospheric teleconnections between both

oceans [*Manabe and Stouffer*, 1988; *Mikolajewicz et al*., 1997; *Schiller et al*., 1997; *Vellinga and Wood*, 2002; *Okumura et al*., 2009; *Chikamoto et al*., 2012; *Max et al*., 2012]. Similarity between N-Pacific SST and the climate evolution in the N-Atlantic realm since approximately the B/A was also described in the Sea of Okhotsk [e.g., *Max et al*., 2012], the NE Pacific [e.g., *Kienast and McKay*, 2001; *Pisias et al*., 2001; *Barron et al*., 2003; *Praetorius and Mix*, 2014; *Praetorius et al*., 2015], and the Bering Sea [*Caissie et al*., 2010; *Max et al*., 2012] and may indicate that atmospheric teleconnections with the N-Atlantic were a widespread control on SST in the N-Pacific and its marginal seas. During HS1, SST_{TEXL86} from the Western Bering Sea resemble NGRIP-$\delta^{18}O$ and reveal a cooling consistent with Heinrich Event 1 (17–16 ka B.P.; Figure 4), indicating that this atmospheric linkage has already been present during the early deglaciation. Heinrich-equivalent cooling in the Bering Sea is in agreement with pronounced sea ice coverage in the region [*Smirnova et al*., 2015; *Méheust et al*., 2015] corroborating the hypothesis that in-phase surface cooling in the N-Pacific and the N-Atlantic fostered NPIW-formation in the Bering Sea through increased brine rejection during sea ice formation [*Rella et al*., 2012; *Riethdorf et al*., 2013; *Max et al*., 2014].

In the NW Pacific (site 12KL), a gradual, uninterrupted increase in SST_{TEXL86} between 18 and 15.5 ka does not agree with the N-Atlantic climate evolution and the SST development in the Western Bering Sea (Figure 4). As the warming in SST_{TEXL86} at site 12KL during the late glacial/HS1 follows the trends of mean summer insolation and CO_{2atm} (Figure 4) it seems likely that those were important factor driving the SST evolution during this time. These regional differences between the NW Pacific and the Bering Sea contrast model simulations, which investigated the response of the N-Pacific to freshwater perturbations in the N-Atlantic under glacial boundary conditions to explicitly investigate the SST response during HS1 (Model for Interdisciplinary Research on Climate simulation [*Chikamoto et al*., 2012]). The model predicted a clear decrease in SST in the Bering Sea as well as in the entire subarctic N-Pacific as a result of atmospheric teleconnections [*Chikamoto et al*., 2012]. This suggests a widespread sensitivity of NW-Pacific SST to atmospheric teleconnections with N-Atlantic climate change already during the early deglaciation/HS1, while SST_{TEXL86} implies that the SST development in the NW Pacific was apparently less sensitive to an atmospheric teleconnection with the N-Atlantic than the Western Bering Sea. Local climate drivers, which may not accurately be represented in the model simulations, could have caused those regional differences.

5.2.2. Regional Controls on Late Glacial SST in the NW Pacific

The temperature development from the NW Pacific resembles the climate evolution in the Gulf of Alaska (GOA; Figure 4). There, $\delta^{18}O$ records, established on planktonic foraminifera, indicate that the climate of the NE-Pacific developed asynchronously with the N-Atlantic realm during the late glacial/HS1 and became synchronized at approximately 15.5 ka [*Praetorius and Mix*, 2014](Figure 4). Moreover, a $U^{K'}_{37}$-based SST record from the GOA provides evidence for progressive warming during the entire HS1 [*Praetorius et al*., 2015] (Figure 4). The similarity between the GOA records and our data indicates a similar SST evolution in the NW Pacific and the GOA (Figure 4). The asynchroneity between the climate development in the GOA and the N-Atlantic realm prior to 15.5 ka B.P. was explained by a southward displacement of the westerly jet due to expanded ice caps on the American continent [*Praetorius and Mix*, 2014]. However, in case of site 12KL in the NW Pacific, it seems unlikely that a southward shift of the westerly jet accounted for the decoupling since an atmospheric connection is suggested by SST_{TEXL86} from the Western Bering Sea, north of site 12KL (Figures 1 and 4). Instead, the similar trends in the GOA records and SST_{TEXL86} suggest the existence of an oceanographic linkage between the eastern and western basin of the subarctic N-Pacific through the Alaskan Stream (AS; Figure 1), which could have been more relevant to the NW Pacific SST than any atmospheric linkage with the N-Atlantic. The proposed east-west linkage corroborates considerations by *Riethdorf et al.* [2013], who reconstructed subsurface salinity and temperature at site 12KL using $\delta^{18}O$ of the foraminifera *Neogloboquadrina pachyderma* (sin) and found relatively cold and fresh conditions in the NW Pacific during HS1. These authors speculated on advection of low-salinity waters from the AS since the Alaskan Current/Alaskan Stream current system experienced drops in salinity due to continental runoff and intensified ice-berg calving, associated with the beginning retreat of continental ice caps during HS1 [*Gebhardt et al*., 2008; *Hendy and Cosma*, 2008; *Taylor et al*., 2014]. By comparing the $\delta^{18}O$ records from the NW Pacific and the GOA this idea is supported as the NW Pacific-$\delta^{18}O$ shows a similar development as the GOA-$\delta^{18}O$ with relatively stable values until 16 ka B.P. followed by a decreasing trend through the late HS1 (Figure 4). So the similar developments of temperature and salinity strongly argue for pronounced influence of the AS on the upper-ocean conditions and the climate in the NW Pacific during the early deglaciation.

5.2.3. Surface Circulation Changes and Long-Term SST Evolution

Considering that sites 114KL and 12KL are under the influence of the EKC, which flows southward along Kamchatka (Figure 1), a similar SST development would be expected for these core sites if the EKC were the dominating influence at both locations throughout the entire glacial to Holocene period. Yet SST developments at sites 12KL and 114KL were dissimilar before 15.5 ka, although the EKC was active during the glacial, attested by deposition of IRD originating from Kamchatka and coastal Siberia in the open NW Pacific Ocean (sites Ocean Drilling Program Site 882, MD01-2412 [*St. John and Krissek*, 1999; *Gebhardt et al*., 2008]). Thus, the AS seems to have dominated over the EKC during the glacial and at least the early deglaciation.

The relative influence of the two surface currents seems to have changed over the deglaciation as our SST_{TEXL86} from site 12KL differs from the GOA-$\delta^{18}O$ and the GOA-$U^{K'}_{37}$ during the Holocene (Figure 4). While in the NW Pacific, SST_{TEXL86} progressively decreases over the Holocene following the trend of mean summer insolation (Figure 4), the GOA records show relatively constant values throughout the Holocene [*Praetorius and Mix*, 2014; *Praetorius et al*., 2015] and resemble the trend of CO_{2atm} (Figure 4). The different SST patterns imply that the influence of the AS on the NW Pacific SST weakened over the deglaciation, likely disconnecting the NW Pacific SST from the NE Pacific. Also, the thermal difference between the Western Bering Sea and the NW Pacific becomes smaller over the deglaciation and the two SST_{TEXL86} records eventually show equal values during the early Holocene (since approximately 11 ka B.P.; Figure 4). Similar SST along the transect points to increased advection of Bering Sea waters into the NW Pacific and thus an increased influence of the EKC. This inference is in agreement with diatom assemblages from site 12KL, which indicate increased influence of coastal Bering Sea waters since approximately 11 ka B.P. [*Smirnova et al*., 2015]. However, our suggested development of the relative intensities of the AS and EKC contrasts conclusions by *Katsuki and Takahashi* [2005]. Analyzing diatom assemblages in the southwestern Bowers Ridge and the open NW Pacific (site ES; Figure 1), these authors found indication for an opposite pattern with a strengthened EKC and a weakened AS during glacial times and vice versa during interglacials. Yet they pointed out that the deglacial changes in the diatom assemblage could also attest to variations in nutrient-availability in the surface layer. This may explain the discrepancies with the conclusions reached in our study.

The change in the relative intensities of the EKC and AS, as elaborated in our study (AS strong during glacials, EKC more influential during the Holocene) may explain the relatively low thermal difference between the glacial and the Holocene SST_{TEXL86} at site 12KL. The increasing intensity of the relatively cold EKC and the concurrent reduction of the relatively warm AS may have buffered the impact of insolation and CO_{2atm} in the NW Pacific.

5.2.4. Causes for Circulation Changes

GCMs suggest that LGM surface temperatures over the subarctic N-Pacific were 0–2°C warmer than at present as the subarctic gyres intensified during the LGM [*Otto-Bliesner et al*., 2006]. This scenario might account for the relatively strong AS during the glacial and hence for the dampened magnitude in SST_{TEXL86} of the NW Pacific (Figures 3 and 4). However, several temperature records from the NE Pacific and Alaska challenge the idea of increased efficiency of the subarctic gyres and increased oceanic heat transport since they point to rather cold LGM conditions [e.g., *Kiefer and Kienast*, 2005; *Praetorius and Mix*, 2014; *Maier et al*., 2015; *Praetorius et al*., 2015]. Alternatively, glacial accumulation of AS waters in the NW Pacific may result from the glacial sea level lowstand since the inflow of AS waters into the eastern Bering Sea decreased during the glacial (relative to the Holocene) when Unimak Pass, the main pathway of the AS into the Bering Sea, and other shallow passages between the Aleutian Islands were closed due to lowered sea level and glaciers expanding over the Islands [*Katsuki and Takahashi*, 2005; *Tanaka and Takahashi*, 2005]. The reduced net inflow of AS waters into the Bering Sea would have consequentially increased the influence of AS waters in the NW Pacific. At the same time the reduced inflow of AS waters into the Eastern and Southern Bering Sea would have limited the influence of the N-Pacific there. The latter might have caused a climatic isolation of the Bering Sea, which would explain why the marginal sea was sensitive to atmospheric teleconnections with the N-Atlantic throughout the entire deglaciation. Unimak Pass opened between 12 and 11 ka B.P. as inferred from fractional abundances of diatoms which point to increased inflow of AS-waters into the southeastern Bering Sea (site 51-JPC, near Unimak Pass; Figure 1) at that time [*Katsuki et al*., 2004; *Caissie et al*., 2010]. This timing is congruent with the beginning deviation of SST_{TEXL86} and GOA records and hence with the interruption of the climatic linkage between the eastern and western subarctic N-Pacific (Figure 4). This coincidence strongly argues for a causal relation between the AS weakening and sea level rise. Therefore, we

consider sea level to be more likely as driver for the surface-circulation changes than increased heat transport in the subarctic gyres.

6. Summary and Conclusions

In order to investigate the SST evolution throughout the entire LGM-Holocene transition, and particularly during HS1 and the LGM, we established TEX^{L}_{86}-based SST records for the Western Bering Sea and the marginal NW Pacific.

SST_{TEXL86} is slightly warmer than existing $SST_{UK'37}$, likely due to different production seasons of Thaumarchaeota (summer) and coccolithophores (fall). Seasonal contrasts were greater during the deglaciation than during the Holocene, which may have resulted from shorter (glacial) summers and/or a stronger Aleutian Low during the glacial and deglaciation, relative to the Holocene. Long-term warming through the LGM-Holocene transition is in accordance with rising CO_{2atm} and summer insolation. The magnitude of deglacial warming in the NW Pacific SST_{TEXL86} was likely dampened by a sea level induced shift in the strengths of the relatively warm AS and the cold EKC, consisting of a relatively strong AS and a weak EKC during the LGM and deglaciation, and vice versa during the Holocene (since approximately 12–11 ka B.P.).

Greenland-like millennial-scale oscillations in SST_{TEXL86} agree with the existing $SST_{UK'37}$, corroborating the hypothesis of an in-phase climate evolution in the N-Atlantic and the N-Pacific due to atmospheric teleconnections. SST_{TEXL86} suggests that such atmospheric coupling has already existed during the early deglaciation (that is HS1) but was likely restricted to the Western Bering Sea as in the NW Pacific a coupling with the N-Atlantic did not establish before approximately 15.5 ka B.P., like in the GOA. Prior to this time SST evolution in the NW Pacific seems to have been driven by CO_{2atm} and summer insolation and was likely linked to the climate development in the GOA through the relatively strong AS. The climatic east-west linkage was interrupted when the AS weakened as a result of the opening of Unimak Pass at the YD/Holocene transition, allowing for different climate developments in the eastern and western N-Pacific throughout the Holocene.

Acknowledgments

The study resulted from core material that was gained in the frame of the German-Russian research project "KALMAR"—Kurile-Kamchatka and Aleutian Marginal Sea Island Arc Systems: Geodynamic and Climate Interaction in Space and Time." We thank the Master and the crew of R/V *SONNE* for their professional support during cruise SO201-2. Dirk Nürnberg is thanked for providing sample material from site SO201-2-12KL. We acknowledge Alexander Weise for his assistance on the geochemical sample preparation. We thank two reviewers for their constructive comments which helped to improve the manuscript. The study was part of a PhD project funded by the Helmholtz association through the President's Initiative and Networking Fund and is supported by GLOMAR—Bremen International Graduate School for Marine Sciences. The data of this study are available on the database "Pangaea" (www.pangaea.de).

References

Alder, J. R., and S. W. Hostetler (2015), Global climate simulations at 3000-year intervals for the last 21,000 years with the GENMOM coupled atmosphere–ocean model, *Clim. Past*, *11*(3), 449–471, doi:10.5194/cp-11-449-2015.

Barron, J. A., L. Heusser, T. Herbert, and M. Lyle (2003), High-resolution climatic evolution of coastal northern California during the past 16,000 years, *Paleoceanography*, *18*(1), 1020, doi:10.1029/2002PA000768.

Berger, A., and M. F. Loutre (1991), Insolation values for the climate of the last 10 million years, *Quat. Sci. Rev.*, *10*(4), 297–317, doi:10.1016/0277-3791(91)90033-Q.

Biskaborn, B. K., U. Herzschuh, D. Bolshiyanov, L. Savelieva, and B. Diekmann (2012), Environmental variability in northeastern Siberia during the last ~13,300 yr inferred from lake diatoms and sediment-geochemical parameters, *Palaeogeogr. Palaeoclimatol. Palaeoecol.*, *329–330*, 22–36, doi:10.1016/j.palaeo.2012.02.003.

Caissie, B. E., J. Brigham-Grette, K. T. Lawrence, T. D. Herbert, and M. S. Cook (2010), Last Glacial Maximum to Holocene sea surface conditions at Umnak Plateau, Bering Sea, as inferred from diatom, alkenone, and stable isotope records, *Paleoceanography*, *25*, PA1206, doi:10.1029/2008PA001671.

Chen, W., M. Mohtadi, E. Schefuß, and G. Mollenhauer (2014), Organic-Geochemical proxies for sea surface temperature in surface sediments in the tropical eastern Indian Ocean, *Deep Sea Res., Part I*, *88*, 17–29, doi:10.1016/j.dsr.2014.03.005.

Chikamoto, M. O., L. Menviel, A. Abe-Ouchi, R. Ohgaito, A. Timmermann, Y. Okazaki, N. Harada, A. Oka, and A. Mouchet (2012), Variability in North Pacific intermediate and deep water ventilation during Heinrich events in two coupled climate models, *Deep Sea Res., Part II*, *61–64*, 114–126, doi:10.1016/j.dsr2.2011.12.002.

Dong, B., and P. J. Valdes (1998), Simulations of the Last Glacial Maximum climates using a general circulation model: Prescribed versus computed sea surface temperatures, *Clim. Dyn.*, *14*(7–8), 571–591, doi:10.1007/s003820050242.

Dullo, W. C., B. Baranov, and C. van den Bogaard (2009), FS Sonne Fahrtbericht/Cruise Report SO201–2. *IFM-GEOMAR, Rep. 35*, 233 pp., IFM-GEOMAR, Kiel, Germany.

Gebhardt, H., M. Sarnthein, P. M. Grootes, T. Kiefer, H. Kuehn, F. Schmieder, and U. Röhl (2008), Paleonutrient and productivity records from the subarctic North Pacific for Pleistocene glacial terminations I to V, *Paleoceanography*, *23*, PA4212, doi:10.1029/2007PA001513.

Harada, N., K. H. Shin, A. Murata, M. Uchida, and T. Nakatani (2003), Characteristics of alkenones synthesized by a bloom of Emiliania huxleyi in the Bering Sea, *Geochim. Cosmochim. Acta*, *67*(8), 1507–1519, doi:10.1016/S0016-7037(02)01318-2.

Harada, N., et al. (2012), Sea surface temperature changes in the Okhotsk Sea and adjacent North Pacific during the last glacial maximum and deglaciation, *Deep Sea Res., Part II*, *61–64*, 93–105, doi:10.1016/j.dsr2.2011.12.007.

Hendy, I. L., and T. Cosma (2008), Vulnerability of the Cordilleran Ice Sheet to iceberg calving during late quaternary rapid climate change events, *Paleoceanography*, *23*, PA2101, doi:10.1029/2008PA001606.

Ho, S. L., et al. (2014), Appraisal of TEX_{86} and thermometries in subpolar and polar regions, *Geochim. Cosmochim. Acta*, *131*, 213–226, doi:10.1016/j.gca.2014.01.001.

Hopmans, E. C., J. W. Weijers, E. Schefuß, L. Herfort, J. S. Sinninghe Damsté, and S. Schouten (2004), A novel proxy for terrestrial organic matter in sediments based on branched and isoprenoid tetraether lipids, *Earth Planet. Sci. Lett.*, *224*(1–2), 107–116, doi:10.1016/j.epsl.2004.05.012.

Karner, M. B., E. F. Delong, and D. M. Karl (2001), Archaeal dominance in the mesopelagic zone of the Pacific Ocean, *Nature*, *409*(6819), 507–510, doi:10.1038/35054051.

Katsuki, K., and K. Takahashi (2005), Diatoms as paleoenvironmental proxies for seasonal productivity, sea-ice and surface circulation in the Bering Sea during the late Quaternary, *Deep Sea Res., Part II*, *52*, 2110–2130, doi:10.1016/j.dsr2.2005.07.001.

Katsuki, K., K. Takahashi, and K. Matsushita (2004), Diatom paleoceanography during the past 340 kyr in the Bering Sea and the western subarctic Pacific, in *Seventeenth International Diatom Symposium*, edited by M. Poulin, pp. 147–159, Biopress, Bristol, U. K.

Kiefer, T., and M. Kienast (2005), Patterns of deglacial warming in the Pacific Ocean: A review with emphasis on the time interval of Heinrich event 1, *Quat. Sci. Rev.*, *24*(7–9), 1063–1081, doi:10.1016/j.quascirev.2004.02.021.

Kienast, S. S., and J. L. McKay (2001), Sea surface temperatures in the subarctic northeast Pacific reflect millennial-scale climate oscillations during the last 16 kyr, *Geophys. Res. Lett.*, *28*(8), 1563–1566, doi:10.1029/2000GL012543.

Kim, J.-H., J. van der Meer, S. Schouten, P. Helmke, V. Willmott, F. Sangiorgi, N. Koç, E. C. Hopmans, and J. S. Sinninghé Damsté (2010), New indices and calibrations derived from the distribution of crenarchaeal isoprenoid tetraether lipids: Implications for past sea surface temperature reconstructions, *Geochim. Cosmochim. Acta*, *74*(16), 4639–4654, doi:10.1016/j.gca.2010.05.027.

Knudson, K. P., and A. C. Ravelo (2015), North Pacific Intermediate Water circulation enhanced by closure of the Bering Strait, *Paleoceanography*, *30*, 1287–1304, doi:10.1002/2015PA002840.

Könneke, M., A. E. de la Torre, J. R. Walker, J. B. Waterbury, and D. A. Stahl (2005), Isolation of an autotrophic ammonia-oxidizing marine archaeon, *Nature*, *437*(7058), 543–546, doi:10.1038/nature03911.

Kuehn, H., L. Lembke-Jene, R. Gersonde, O. Esper, F. Lamy, A. Arz, G. Kuhn, and R. Tiedemann (2014), Laminated sediments in the Bering Sea reveal atmospheric teleconnections to Greenland climate on millennial to decadal timescales during the last deglaciation, *Clim. Past*, *10*(6), 2215–2236, doi:10.5194/cp-10-2215-2014.

Locarnini, R. A., A. V. Mishonov, J. I. Antonov, T. P. Boyer, H. E. Garcia, O. K. Baranova, M. M. Zweng, and D. R. Johnson (2010), World Ocean Atlas 2009: Volume 1: Temperature, in *NOAA Atlas NESDIS 68*, edited by S. Levitus, pp. 184, U.S. Gov. Print. Off., Washington, D.C.

Maier, E., M. Méheust, A. Abelmann, R. Gersonde, B. Chapligin, J. Ren, J. R. Stein, H. Meyer, and R. Tiedemann (2015), Deglacial subarctic Pacific surface water hydrography and nutrient dynamics and links to North Atlantic climate variability and atmospheric CO_2, *Paleoceanography*, *30*, 949–968, doi:10.1002/2014PA002763.

Manabe, S., and R. J. Stouffer (1988), Two stable equilibria of a coupled ocean-atmosphere model, *J. Clim.*, *1*(9), 841–861, doi:10.1175/1520-0042(1988)001<0841:TSEOAC>2.0.CO;2.

Martens-Habbena, W., P. M. Berube, H. Urakawa, J. R. de la Torre, and D. A. Stahl (2009), Ammonia oxidation kinetics determine niche separation of nitrifying Archaea and Bacteria, *Nature*, *461*(7266), 976–979, doi:10.1038/nature08465.

Max, L., J.-R. Riethdorf, R. Tiedemann, M. Smirnova, L. Lembke-Jene, K. Fahl, D. Nürnberg, A. Matul, and G. Mollenhauer (2012), Sea surface temperature variability and sea-ice extent in the subarctic northwest Pacific during the past 15,000 years, *Paleoceanography*, *27*, PA3213, doi:10.1029/2012PA002292.

Max, L., L. Lembke-Jene, J.-R. Riethdorf, R. Tiedemann, D. Nürnberg, H. Kühn, and A. Mackensen (2014), Pulses of enhanced North Pacific Intermediate Water ventilation from the Okhotsk Sea and Bering Sea during the last deglaciation, *Clim. Past*, *10*(2), 591–605, doi:10.5194/cp-10-591-2014.

McManus, J. F., R. Francois, J. M. Gherardi, L. D. Keigwin, and S. Brown-Leger (2004), Collapse and rapid resumption of Atlantic meridional circulation linked to deglacial climate change, *Nature*, *428*(6985), 834–837, doi:10.1038/nature02494.

Méheust, M., R. Stein, K. Fahl, L. Max, and J.-R. Riethdorf (2015), High-resolution IP25-based reconstruction of sea-ice variability in the western North Pacific and Bering Sea during the past 18,000 years, *Geo Mar. Lett.*, doi:10.1007/s00367-015-0432-4.

Menviel, L., A. Timmermann, O. Elison Timm, A. Mouchet, A. Abe-Ouchi, M. O. Chikamoto, N. Harada, R. Ohgaito, and Y. Okazaki (2012), Removing the North Pacific halocline: Effects on global climate, ocean circulation and the carbon cycle, *Deep Sea Res., Part II*, *61–64*, 106–113, doi:10.1016/j.dsr2.2011.03.005.

Mikolajewicz, U., T. J. Crowley, A. Schiller, and R. Voss (1997), Modelling teleconnections between the North Atlantic and North Pacific during the Younger Dryas, *Nature*, *387*(6631), 384–387, doi:10.1038/387384a0.

Monnin, E., A. Indermühle, A. Dällenbach, J. Flückiger, B. Stauffer, T. F. Stocker, D. Raynaud, and J. M. Barnola (2001), Atmospheric CO_2 concentrations over the last glacial termination, *Science*, *291*(5501), 112–114, doi:10.1126/science.291.5501.112.

Niebauer, H. J., N. A. Bond, L. P. Yakunin, and V. V. Plotnikov (1999), An update on the climatology and sea ice of the Bering Sea, in *Dynamics of the Bering Sea*, edited by T. R. Loughlin and K. Ohtani, pp. 29–59, Univ. Alaska Sea Grant, Fairbanks, doi:10.1029/2003GC000559.

North Greenland Ice Core Project members (2004), High-resolution record of northern hemisphere climate extending into the last interglacial period, *Nature*, *431*(7005), 147–151, doi:10.1038/nature02805.

Ohtani, K., Y. Akiba, and A. Y. Takenouti (1972), Formation of western subarctic water in the Bering Sea, in *Biological Oceanography of the Northern North Pacific Ocean*, edited by A. Y. Takenouti, pp. 32–44, Idemitsu Shoten Publ. Co, Tokyo, doi:10.1029/2003GC000559.

Okazaki, Y., A. Timmermann, L. Menviel, N. Harada, A. Abe-Ouchi, M. O. Chikamoto, A. Mouchet, and H. Asahi (2010), Deepwater formation in the North Pacific during the Last Glacial Termination, *Science*, *329*(5988), 200–204, doi:10.1016/j.dsr2.2005.07.003.

Okumura, Y. M., C. Deser, A. Hu, A. Timmermann, and S.-P. Xie (2009), North Pacific climate response to freshwater forcing in the subarctic North Atlantic: Oceanic and atmospheric pathways, *J. Clim.*, *22*(6), 1424–1445, doi:10.1175/2008JCLI2511.1.

Otto-Bliesner, B. L., E. C. Brady, G. Clauzet, R. Tomas, S. Levis, and Z. Kothavala (2006), Last glacial maximum and Holocene climate in CCSM3, *J. Clim.*, *19*(11), 2526–2544, doi:10.1175/JCLI3748.1.

Parrenin, F., V. Masson-Delmotte, P. Köhler, D. Raynaud, D. Paillard, J. Schwander, C. Barbante, A. Landais, A. Wegener, and J. Jouzel (2013), Synchronous change of atmospheric CO_2 and Antarctic temperature during the last deglacial warming, *Science*, *339*(6123), doi:10.1126/science.1226368.

Pisias, N., A. Mix, and L. Heusser (2001), Millennial scale climate variability of the northeast Pacific Ocean and northwest North America based on radiolaria and pollen, *Quat. Sci. Rev.*, *20*(14), 1561–1576, doi:10.1016/SO277-3791(01)0018-X.

Praetorius, S. K., and A. C. Mix (2014), Synchronization of North Pacific and Greenland climates preceded abrupt deglacial warming, *Science*, *345*(6196), 444–448, doi:10.1126/science.1252000.

Praetorius, S. K., A. C. Mix, M. H. Walczak, M. D. Wolhowe, J. A. Addison, and F. G. Prahl (2015), North Pacific deglacial hypoxic events linked to abrupt ocean warming, *Nature*, *527*(7578), 362–366, doi:10.1038/nature15753.

Rella, S. F., R. Tada, K. Nagashima, M. Ikehara, T. Itaki, K. Ohkushi, T. Sakamoto, N. Harada, and M. Uchida (2012), Abrupt changes of intermediate water properties on the northeastern slope of the Bering Sea during the last glacial and deglacial period, *Paleoceanography*, *27*, PA002205, doi:10.1029/2011PA002205.

Riethdorf, J.-R., L. Max, D. Nürnberg, L. Lembke-Jene, and R. Tiedemann (2013), Deglacial development of (sub) sea surface temperature and salinity in the subarctic northwest Pacific: Implications for upper-ocean stratification, *Paleoceanography*, *28*, 91–104, doi:10.1002/palo.20014.

Saenko, O. A., A. Schmittner, and A. J. Weaver (2004), The Atlantic–Pacific Seesaw, *J. Clim.*, *17*(11), 2033–2038, doi:10.1175/1520-0442(2004)017<2033:TAS>2.0CO;2.

Sarnthein, M., H. Gebhardt, T. Kiefer, M. Kucera, M. Cook, and H. Erlenkeuser (2004), Mid Holocene origin of the sea-surface salinity low in the subarctic North Pacific, *Quat. Sci. Rev.*, *23*(20–22), 2089–2099, doi:10.1016/j.quascirev.2004.08.008.

Sarnthein, M., T. Kiefer, P. M. Grootes, H. Elderfield, and H. Erlenkeuser (2006), Warmings in the far northwestern Pacific promoted pre-Clovis immigration to America during Heinrich event 1, *Geology*, *34*(3), 141, doi:10.1130/G22200.1.

Schiller, A., U. Mikolajewicz, and R. Voss (1997), The stability of the North Atlantic thermohaline circulation in a coupled ocean-atmosphere general circulation model, *Clim. Dyn.*, *13*(5), 325–347, doi:10.1007/s003820050169.

Schlitzer, R. (2011), Ocean Data View. [Available at http://odv.awi.de.]

Schmittner, A., O. A. Saenko, and A. J. Weaver (2003), Coupling of the hemispheres in observations and simulations of glacial climate change, *Quat. Sci. Rev.*, *22*(5–7), 659–671, doi:10.1016/S0277-3791(02)00184-1.

Schouten, S., E. C. Hopmans, E. Schefuß, and J. S. Sinninghe Damsté (2002), Distributional variations in marine crenarchaeotal membrane lipids: A new tool for reconstructing ancient sea water temperatures?, *Earth Planet. Sci. Lett.*, *204*(1–2), 265–274, doi:10.1016/S0012-821X(02)00979-2.

Seki, O., R. Ishiwatar, and K. Matsumoto (2002), Millennial climate oscillations in NE Pacific surface waters over the last 82 kyr: New evidence from alkenones, *Geophys. Res. Lett.*, *29*(23), 2144, doi:10.1029/2002GL015200.

Seki, O., K. Kawamura, M. Ikehara, T. Nakatsuka, and T. Oba (2004a), Variation of alkenone sea surface temperature in the Sea of Okhotsk over the last 85 kyr, *Org. Geochem.*, *35*(3), 347–354, doi:10.1016/j.orggeochem.2003.10.011.

Seki, O., M. Ikehara, K. Kawamura, T. Nakatsuka, K. Ohnishi, M. Wakatsuchi, H. Narita, and T. Sakamoto (2004b), Reconstruction of paleoproductivity in the Sea of Okhotsk over the last 30 kyr, *Paleoceanography*, *19*, PA1016, doi:10.1029/2002PA000808.

Seki, O., T. Nakatsuka, K. Kawamura, S.-I. Saitoh, and M. Wakatsuchi (2007), Time-series sediment trap record of alkenones from the western Sea of Okhotsk, *Mar. Chem.*, *104*(3–4), 253–265, doi:10.1016/j.marchem.2006.12.002.

Seki, O., T. Sakamoto, S. Sakai, S. Schouten, E. C. Hopmans, S. J. Sinninghe Damste, and R. D. Pancost (2009), Large changes in seasonal sea ice distribution and productivity in the Sea of Okhotsk during the deglaciations, *Geochem. Geophys. Geosyst.*, *10*, Q10007, doi:10.1029/2009GC002613.

Seki, O., J. A. Bendle, N. Harada, M. Kobayashi, K. Sawada, H. Moossen, G. N. Inglis, S. Nagao, and T. Sakamoto (2014), Assessment and calibration of TEX_{86} paleothermometry in the Sea of Okhotsk and sub-polar North Pacific region: Implications for paleoceanography, *Prog. Oceanogr.*, *126*, 254–266, doi:10.1016/j.pocean.2014.04.013.

Shin, S. I., Z. Liu, B. Otto-Bliesner, E. C. Brady, J. E. Kutzbach, and S. P. Harrison (2003), A simulation of the Last Glacial Maximum climate using the NCAR-CCSM, *Clim. Dyn.*, *20*(2–3), 127–151, doi:10.1007/s00382-002-0260-x.

Smirnova, M. A., G. K. Kazarina, A. G. Matul, and L. Max (2015), Diatom evidence for paleoclimate changes in the northwestern Pacific during the last 20,000 years, *Mar. Geol.*, *55*(3), 425–431, doi:10.1134/S0001437015030157.

St. John, K. E. K., and L. A. Krissek (1999), Regional patterns of Pleistocene ice-rafted debris flux in the North Pacific, *Paleoceanography*, *14*(5), 653–662, doi:10.1029/1999PA900030.

Stabeno, P. J., and R. K. Reed (1994), Circulation in the Bering Sea basin by satellite tracked drifters, *J. Phys. Oceanogr.*, *24*(4), 848–854.

Takahashi, K., N. Fujitani, and M. Yanada (2002), Long term monitoring of particle fluxes in the Bering Sea and the central subarctic Pacific Ocean, 1990-2000, *Prog. Oceanogr.*, *55*(1–2), 95–112, doi:10.1016/S0079-6611(02)00072-1.

Tanaka, S., and K. Takahashi (2005), Late Quaternary paleoceanographic changes in the Bering Sea and the western subarctic Pacific based on radiolarian assemblages, *Deep Sea Res., Part II*, *52*(16–18), 2131–2149, doi:10.1016/j.dsr2.2005.07.002.

Taylor, M. A., I. L. Hendy, and D. K. Pak (2014), Deglacial ocean warming and marine margin retreat of the Cordilleran Ice Sheet in the North Pacific Ocean, *Earth Planet. Sci. Lett.*, *403*, 89–98, doi:10.1016/j.epsl.2014.06.026.

Ternois, Y., K. Kawamura, N. Ohkouchi, and L. Keigwin (2000), Alkenone sea surface temperature in the Okhotsk Sea for the last 15 kyr, *Geochem. J.*, *34*(4), 283–293, doi:10.2343/geochemj.34.283.

Timmermann, A., L. Menviel, Y. Okumura, A. Schilla, U. Merkel, O. Timm, A. S. Hu, B. Otto-Bliesner, and M. Schulz (2010), Towards a quantitative understanding of millennial scale Antarctic warming events, *Quat. Sci. Rev.*, *29*(1–2), 74–85.

Vellinga, M., and R. A. Wood (2002), Global climate impacts of a collapse of the Atlantic thermohaline circulation, *Clim. Change*, *54*(3), 251–267, doi:10.1023/A:1016168827653.

Waelbroeck, C., et al. (2009), Constraints on the magnitude and patterns of ocean cooling at the Last Glacial Maximum, *Nat. Geosci.*, *2*, 127–132, doi:10.1038/ngeo411.

Walker, C. B., et al. (2010), Nitrosopumilus maritimus genome reveals unique mechanisms for nitrification and autotrophy in globally distributed marine Crenarchaea, *Proc. Natl. Acad. Sci. U.S.A.*, *107*, 8818–8823, doi:10.1073/pnas.0913533107.

Weijers, J. W. H., S. Schouten, O. C. Spaargaren, and J. S. Sinninghe Damsté (2006), Occurrence and distribution of tetraether membrane lipids in soils: Implications for the use of the TEX_{86} proxy and the BIT index, *Org. Geochem.*, *37*(12), 1680–1693, doi:10.1016/j.orggeochem.2006.07.018.

Yamamoto, M., A. Shimamoto, T. Fukuhara, Y. Tanaka, and J. Ishizaka (2012), Glycerol dialkyl glycerol tetraethers and TEX_{86} index in sinking particles in the western North Pacific, *Org. Geochem.*, *53*, 52–62, doi:10.1016/j.orggeochem.2012.04.010.

Yanase, W., and A. Abe-Ouchi (2007), The LGM surface climate and atmospheric circulation over East Asia and the North Pacific in the PMIP2 coupled model simulations, *Clim. Past.*, *3*(3), 439–451, doi:10.5194/cp-3-439-2007.

Yanase, W., and A. Abe-Ouchi (2010), A numerical study on the atmospheric circulation over the midlatitude North Pacific during the last glacial maximum, *J. Clim.*, *23*(1), 135–151, doi:10.1175/2009JCLI3148.1.